Title	The effect of feedstock origin and temperature on the structure and reactivity of char from pyrolysis at 1300 2800 °C
Author(s)	Surup, Gerrit Ralf; Foppe, Manuel; Schubert, Daniel; Deike, Rüdiger; Heidelmann, Markus; Timko, Michael T.; Trubetskaya, Anna
Publication Date	2018-07-31
Publication Information	Surup, Gerrit Ralf, Foppe, Manuel, Schubert, Daniel, Deike, Rüdiger, Heidelmann, Markus, Timko, Michael T., & Trubetskaya, Anna. (2019). The effect of feedstock origin and temperature on the structure and reactivity of char from pyrolysis at 1300–2800°C. Fuel, 235, 306-316. doi: https://doi.org/10.1016/j.fuel.2018.07.093
Publisher	Elsevier
Link to publisher's version	https://doi.org/10.1016/j.fuel.2018.07.093
Item record	http://hdl.handle.net/10379/7451
DOI	http://dx.doi.org/10.1016/j.fuel.2018.07.093

The effect of feedstock origin and temperature on the structure and reactivity of char from pyrolysis at 1300-2800°C

Gerrit Ralf Surup[a], Manuel Foppe[b], Daniel Schubert[b], Rüdiger Deike[b], Markus Heidelmann[c], Michael T Timko[d], Anna Trubetskaya[e,*]

[a]*Department of Engineering Sciences, University of Agder, 4879 Grimstad, Norway*
[b]*Chair of Metallurgy for Iron and Steel Production, University of Duisburg-Essen, 47119 Duisburg, Germany*
[c]*Interdisciplinary Center for Analytics on the Nanoscale, University of Duisburg-Essen, 47057 Duisburg, Germany*
[d]*Chemical Engineering Department, Worcester Polytechnic Institute, 01609 Worcester, MA, USA*
[e]*Mechanical Engineering Department, National University of Ireland, H91TK33 Galway, Ireland*

Abstract

This study reports the effect of feedstock origin, residence time and heat treatment temperature on CO_2 and O_2 reactivities, nanostructure and carbon chemistry of chars prepared at 1300, 1600, 2400 and 2800°C in a slow pyrolysis reactor. The structure of char was characterized by transmission electron microscopy and Raman spectroscopy. The CO_2 and O_2 reactivity of char was investigated by thermogravimetric analysis. Results showed that the ash composition and residence time influence the char reactivity less than the heat treatment temperature. The heat treatment temperature and co-pyrolysis of pinewood char with biooil decreased the CO_2 reactivity approaching that of metallurgical coke. Importantly from a technological standpoint,

*Corresponding author. anna.trubetskaya@nuigalway.ie

the reactivities of char from high temperature pyrolysis (2400-2800°C) were similar to those of metallurgical coke emphasizing the importance of graphitizing temperatures on the char behavior. Moreover, graphitization of chars from wood and herbaceous biomass increased with the increasing heat treatment temperature, leading to formation of graphitizing carbon.
Keywords: biomass char, high-temperature pyrolysis, reactivity, biooil, metallurgical coke

---

1. Introduction

Ferroalloy production is energy-intensive, consuming large amounts of both electricity and coke. Coke is used in this process to reduce metal oxides naturally present in ores to produce the base metal. Development of cost-effective, renewable reductants is environmentally desirable because global ferroalloy production releases about 55 Mt of CO_2 emissions annually [1]. Using carbon sources from renewable, plant-based feeds has potential to replace fossil-based reducing agents and effectively reduce CO_2 emissions. In recent years, much progress has been made on conversion of plant-based materials to carbonaceous char materials; some of these materials may have potential as reductants. However, metallurgical production continues to rely on fossil-based reductants due to limited knowledge of char properties, knowledge gaps in the conditions required to produce chars with acceptable reactivity, and high costs.

Ferroalloys are defined as iron-rich alloys which contain high proportions of Si, Mn, C, Cr, etc. which improve tensile strength, wear, corrosion resistance and toughness [1]. Ferroalloys are produced in submerged-arc furnaces

at temperatures > 1500°C. Within the furnace, a three-phase electrode inserted into a mixture consisting of metal oxide and carbonaceous reductants, typically metallurgical coke and coal [2]. The carbonaceous materials serve many roles, with the primary function being to reduce the metal oxide to form the base metal [3]. Additionally, the carbonaceous materials improve gas distribution during the reduction process, trap SiO gas, enhance electrical resistance of the reaction mixture [4, 5]. The most important properties of the carbonaceous reductant are high reactivity, high conversion and low levels of impurities (such as sulphur and phosphorus) [6]. Low ash content is important, as each additional percent of ash in carbonaceous reductant increases slag volume by about 10-15 kg t^{-1} of ferroalloy, thereby increasing the electric power required for smelting [5].

In recent years, many studies investigated production and/or co-production of carbonaceous solids by pyrolysis treatment of wide variety of renewable feedstocks [3, 5, 7–11]. In comparison with the metallurgical coke traditionally used in ferroalloy production, carbon produced from renewable feedstocks contains less fixed carbon and a greater percentage of volatile components and may need to be graphitized prior to use as a reductant [11]. Although different types of biomass can be converted into biochar, herbaceous biomass species are especially promising candidates for the use as carbonaceous reductants in ferroalloy industries because of their high growth rate and relative ease of harvest [7]. Despite these arguments in favor of herbaceous biochars, the majority of previous investigations have studied charcoals produced at temperatures < 1000°C [12–18]. Thus, the effects of feedstock composition, treatment at temperatures greater than > 1250°C,

and residence time on the char reactivity and structure have not been studied in depth. In particular, herbaceous feedstocks contain high amounts of alkali metals which promote faster devolatilization rates and suppress tar formation, leading to higher char yields and higher CO_2/O_2 reactivity than charcoals produced from wood [19]. The high reactivity of biochar reductant may be advantageous in some cases within the ferroalloy industries. However, the use of a reductant more reactive than metallurgical coke may increase maintenance costs due to the decreased electrical conductivity [20, 21]. Therefore, reductant reactivity becomes a key variable that must be understood in potential replacements for metallurgical coke. Likewise, the effect of residual alkali metal content in biochar produced from pyrolysis of herbaceous biomass must be considered. Previous studies report that nearly 50 % potassium in the herbaceous biomass is released in the temperature range from 900-1250°C, with residual potassium likely being present as counter ions in phenolate groups [22, 23]. In addition, alkali metal ions (K^+ and Ca^{2+}) promote catalytic conversion of tars to small molecule products in a temperature range from 700 to 900°C [24]. However, treatment at temperatures greater than 1250°C will be required to produce graphitic or turbostratic carbons suitable as metallurgical coke, and the fate of potassium at these temperatures is not clear. In addition to knowledge gaps in reactivity and composition, the cost of biochar reductants is not competitive with metallurgical coke, in part due to low biochar yields. Previous studies have examined deposition of biooil and tar recycling to increase char yields and to decrease char reactivity [11, 25]. For example, impregnating biooil within an existing char increased the total char yield with minimal effect on char microporosity

and adsorption properties [26]. Similarly, deposition of biooil on biochar prior to pyrolysis promoted formation of oxygen-containing functional groups and transformation of small aromatic rings to larger aromatic rings [27]. However, literature data is scarce that describes the effect of biooil deposition on resulting char properties that impact metallurgical applications, adding uncertainty to the use of biooil impregnation as an approach to increase char yields and decrease char reactivity.

In summary, renewable feeds have potential as environmentally benign replacements to fossil-based reductants used in ferroalloys production, but knowledge of relationships between feedstock, operating conditions, and biochar properties is limited. In this study, the impacts of feedstock, heat treatment temperature (from 1600 to 2800°C), residence time, and nanostructure on the CO_2/O_2 reactivity of woody and herbaceous biomass were investigated. The specific objectives of this study were to: (1) develop structure-property relationships governing the CO_2 and O_2 reactivity of biochar at high-temperatures, and (2) determine the treatment conditions and feedstock composition which decrease char reactivity to levels that are suitable for application in ferroalloy industries.

2. Materials and methods

Pinewood, beechwood, wheat straw, leached wheat straw and alfalfa straw were chosen for the fast pyrolysis study in a drop tube furnace (DTF). The low-ash containing wood (pinewood, beechwood) of syringyl (S) or guaiacyl-syringyl (GS) lignin types and herbaceous biomass (wheat straw, alfalfa straw) of hydroxy phenol-guaiacyl-syringyl (HGS) lignin type, which are rich

in K, Ca and Si elements, were selected to investigate the effect of differences in ash composition and organic matter (cellulose, hemicellulose, lignin, extractives) on the char structure and reactivity. The wheat straw was leached in deionized water (room temperature) by continuous stirring for 12 hours, followed by drying at 30°C in an oven desiccator without any ventilation. Due to leaching of wheat straw, the metal content was reduced to $\approx 60\,\%$ of the original value and the Cl, S, K, Na and P contents were strongly reduced. Char samples were generated in the drop tube reactor at 1250°C, as described in detail by Trubetskaya et al. [28]. The temperature of 1250°C that is the wall temperature of the DTF was selected to ensure the complete pyrolysis. The reactor consists of an alumina tube (internal diameter: 54 mm, heated length: 1.06 m) heated by four heating elements with independent temperature control. The experiments were conducted by feeding $\approx$ 5 g of biomass at a rate of 0.2 g min^{-1}. Both primary (0.18 l min^{-1} measured at 20°C and 101.3 kPa) and secondary (4.8 l min^{-1} measured at 20°C and 101.3 kPa) feed gases were N_2. The residence time of fuel particles was estimated to be about 1 s, taking into account density changes during pyrolysis. The char samples generated at 1250°C were further heated up to 1300, 1600, 2400, and 2800°C in high-temperature furnaces. The effect of residence time on the char properties was studied by keeping samples at 1300 or 1600°C for 2 or 12 h.

Pinewood biooil was supplied by BTG BioLiquids. When used, 10 g of pinewood char mixed with 20 mL of biooil were stirred at 40°C for 5 days and further reacted at 1600°C in a high-temperature furnace. The CO_2 and O_2 reactivity of all char samples was investigated in a thermogravimetric

analyzer. Reactivities of biomass chars and metallurgical coke were compared using reaction rates calculated from the derived kinetic parameters. TEM analysis and Raman spectroscopy were performed to characterize the effect of temperature, residence time, and feedstock on the char carbon chemistry and nanostructure.

2.1. Raw biomass characterization

The ultimate and proximate analysis of pinewood, beechwood, wheat straw, leached wheat straw, alfalfa straw, metallurgical coke and pinewood biooil is shown in Table 1.

Table 1: Proximate and ultimate analysis.

Fuel	Pine-wood	Beech-wood	Wheat straw	Alfalfa straw	Leached wheat straw	Metallur-gical coke	Pinewood biooil[a]
Proximate analysis							
Moisture, (wt. % as received)	5.1	4.5	5.5	5.2	4.3	0.6	25
Ash at 550°C, (wt. % dry basis)	0.3	1.4	4.1	7.4	2.1	11.8	0.01
Volatiles, (wt. % dry basis)	86.6	79.4	77.5	75.9	82.2	3	-
HHV, (MJ kg^{-1})	21.6	20.2	18.8	19.7	19	27.9	18.5
LHV, (MJ kg^{-1})	20.2	19	17.5	16.9	17.2	27.8	16
Ultimate analysis, (wt. %, dry basis)							
C	53.1	50.7	46.6	42.5	46.2	85.6	46
H	6.5	5.9	6.1	6.7	6.8	0.3	7
N	0.06	0.13	0.6	0.3	0.05	1.8	0.01
O	40	41.9	42.5	43.1	44.8		47
S	<0.01	0.01	0.1	0.03	0.02	0.5	0.01
Cl	0.01	0.02	0.1	0.5	0.01	0.03	0.003
Ash compositional analysis, (mg kg^{-1}, dry basis)							
Al	10	10	150	600	100	12000	550
Ca	600	2000	2500	12900	1300	6400	500
Fe	20	10	200	-	350	6300	200
K	200	3600	11000	28000	1200	1700	850
Mg	100	600	750	1400	350	1300	550
Na	30	100	150	1000	50	1100	200
P	6	150	550	1900	80	400	10
Si	50	200	8500	2000	6200	27000	1800
Ti	2	< 8	10	30	10	550	10

[a] kinematic viscosity at 40°C: 13 cSt; pH: 2.9; density: 1.2 kg lt^{-1}; solid content: 0.04 %

The fuels were milled on a Retsch rotor mill RZ200 and sieved to a particle size fraction of 0.2-0.425 mm. The analysis of biomass constituents (cellulose, hemicellulose, acid-soluble lignin, acid-insoluble lignin, and extractives) was conducted according to NREL technical reports [29–31] and Thammasouk et al. [32], and shown in Table 2.

Table 2: Lignocellulosic composition of woody and herbaceous biomass.

Biomass	**Cellulose**	**Hemi-cellulose**	**Lignin**		**Extractives**	**Protein**
			acid insoluble	**acid soluble**		
Pinewood	38.3	17.8	29.6	1.8	8.8*	0.6
Beechwood	35	19.2	32	1.5	7.5*	1.9
Wheat straw	35.9	18	19.2	6.5	10.1**	6.3
Leached wheat straw	32.1	23.5	13.8	2	13.3**	1.3
Alfalfa straw	18.8	12	14.7	6.8	39.6**	5.1

* acetone extraction ** ethanol-water extraction (room temperature)

2.2. High-temperature furnace (1300-2400° C)

The char samples were further treated in the high-temperature furnace LHTG 200-300/20-1G (Carbolite Gero, Germany), as shown in Figure 1. The furnace can be operated at temperatures up to 1800°C and at heating rates up to 20°C min^{-1}. Prior to each experiment, 5 g of the char sample was loaded into the A_2O_3 crucible (Almath Crucibles Ltd, UK) placed in the graphite retort middle. Prior to pyrolysis, the furnace was repeatedly evacuated and purged by argon. The char sample was heated at 10°C min^{-1} up to 1300 and 1600°C and kept at that temperature for 2 h. The sample was cooled to room temperature at a rate of 20°C min^{-1}. Another high-temperature furnace 200-300/30-1G (Carbolite Gero, Germany) was used to heat the char sample to 2400°C. Samples were stored in sealed plastic containers.

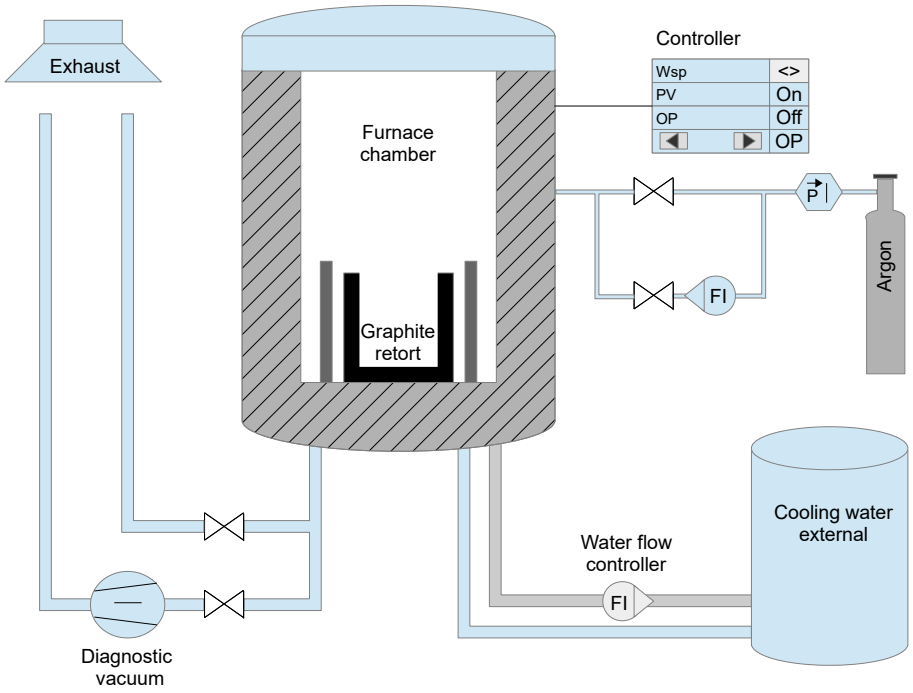

Figure 1: High-temperature furnace at University of Agder.

2.3. High-temperature furnace (2800° C)

The biochar was treated in a vacuum induction furnace (max. 60 kW, max. 10 kHz) with a chamber volume of 0.5 m^3, as shown in Figure 2. The heating vessel consists of a three-part crucible with an outer alumina crucible (outer diameter: 130 mm, inner diameter: 110 mm, height: 300 mm), a middle carbon crucible (outer diameter: 90 mm, inner diameter: 50 mm, height: 145 mm) and an inner glass carbon crucible (outer diameter: 50 mm, inner diameter: 38 mm, height: 125 mm). The three-part crucible was positioned in an induction coil.

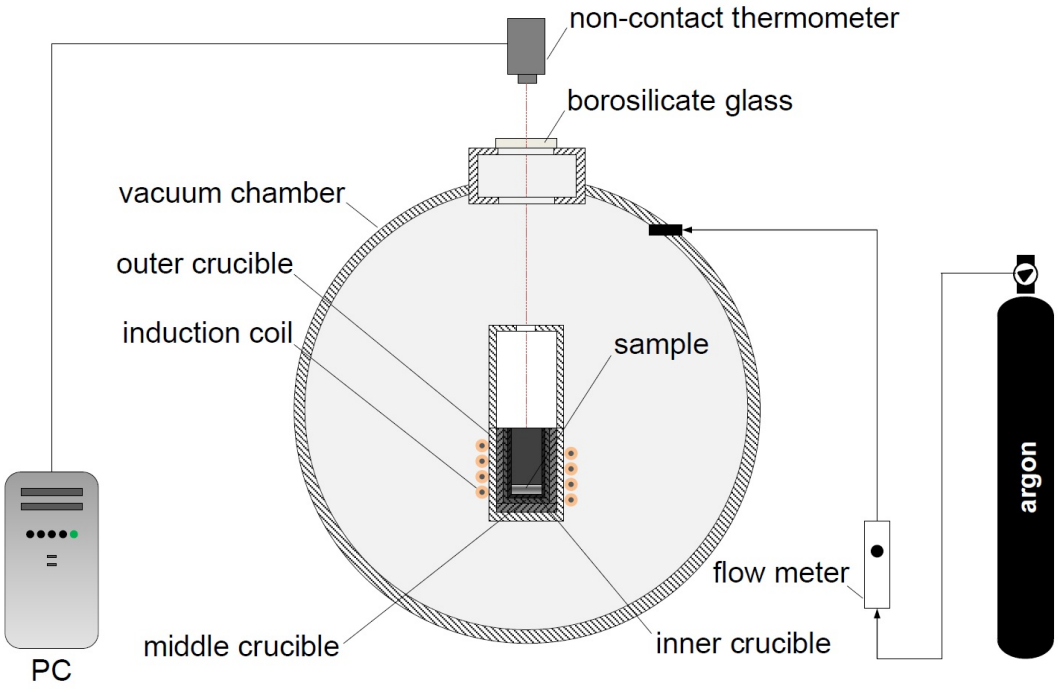

Figure 2: High-temperature furnace at University of Duisburg-Essen.

The gap between the alumina crucible and the carbon crucible was filled up with a carbon felt. A carbon felt disc (diameter: 110 mm, height: 30 mm) between the bottom of alumina and carbon crucibles was used for the high-temperature protection. The sample was placed in the glassy carbon crucible. The sample temperature was measured by a non-contact thermometer (Cyclops 100L 2F, LAND AMETEK) through a borosilicate glass tube (diameter: 180 mm, height: 20 mm) at the upper part of the vacuum chamber. The non-contact thermometer was calibrated against Pt, Al_2O_3, and Mo. Prior to the experiment, the chamber was evacuated and filled with argon. The chamber was continuously purged by argon at a defined flow rate of 10 l min^{-1}. The sample was heated at 3°C s^{-1} up to 2800°C and kept at

that temperature for 2 h. The sample was cooled to room temperature at a heating rate of 30°C min^{-1} and stored in sealed plastic containers.

2.4. Char analysis

Elemental analysis. The elemental analysis was performed on Analyser Series II (Perkin Elmer, USA). Acetanilide was used as a reference standard. The ash content was determined using a standard ash test at 550°C, according to the procedure described in DIN EN 14775.

Thermogravimetric analysis. The char samples were crushed to a fine powder in a mortar with a ceramic pestle. The reactivity of char was analyzed by exposing samples to a reactive gas consisting of 40 % volume fraction CO_2 and 5 % volume fraction O_2 in a thermogravimetric instrument Q600 (TA Instrument, USA). In each experiment, 4 mg of sample were loaded into an Al_2O_3 crucible and heated from 30 to 1500°C in CO_2 at a constant heating rate of 10°C min^{-1}. The kinetic parameters of char samples were derived by the integral method presented by Coats and Redfern [33]. Through integral transformation and mathematical approximation, the linear equation was expressed in the form:

$$ln\left(-\frac{ln(1-X)}{T^2}\right) = ln\left(\frac{A \cdot R}{\kappa \cdot E_a}\right) - \frac{E_a}{R \cdot T} \quad (1)$$

In equation 1, κ is the heating rate and R is the gas constant. A plot of ln(-ln(1-X) T^{-2}) versus T^{-1} gives a straight line whose slope and intercept determine the values of the activation energy (E_a) and pre-exponential factor (A). The reactivities of char samples were compared using reaction rates calculated from the derived kinetic parameters (A and E_a) at a fixed gasification temperature of 1000°C.

Raman spectroscopy. Raman spectroscopy was performed using an inVia Raman microscope (Renishaw, UK) operating with a 514 nm laser line at a power of 30 mW. The measurements were performed in static mode with a center at 1600 cm^{-1}, resulting in a 960-2200 cm^{-1} spectral region. The laser power was set to 100 % in the software and roughly 30 % in the hardware by using a filter. 1 s exposure time was used in normal confocality mode. A 20x lens and 8-15 μm step size (X and Y directions) was used for mapping, to generate 100-200 spectra/image for each char sample. Cosmic rays were removed and the data was subjected to multivariate noise filtering using the WiRE chemometrics package version 3.0 (Renishaw, UK). Spectra were saved as text files and processed via the free, open-source MatLab script provided by the Vibrational Spectroscopy Core Facility at Umeå University (www.kbc.umu.se/english/visp/download-visp/). The following parameters were used for spectra pre-processing: asymmetrical least squares baseline correction with lambda = 20000000 and p = 0.001 [34]; Savitzky-Golay smoothing with the first polynomial order and frame rate of 3 [35]. Spectra were total area normalized in the entire spectral range. The corrected spectra from each mapping were then averaged to create a final composite curve for the peak deconvolution. No spectral scaling was performed. Deconvolution of the Raman spectra was conducted using the peak fit pro tool in the OriginPro software (OriginLab, USA) by combination of seven Gaussian-shaped bands (D_4, D_3, D, D_2, D_5, G, and D_6) following Sadezky et al. [36]. The mean crystal size in the *a*-direction (L_a) with the fitting constants C_0 = -12.6 nm and C_1 = 0.033, which are valid for the laser wavelength from 400 to 700 nm,

is given by [37]:

$$L_a = \frac{C_0 + C_1 \lambda_L}{A_D / A_G} \tag{2}$$

Transmission electron microscopy. Prior to microscopy, char samples were held at 350°C for 6 h in a thermogravimetric instrument to devolatize the samples. Samples were ground in a mortar to ensure a homogeneous particle distribution, sonified in deionized water for 30 min, wet dispersed on a lacey carbon copper grid and dried at room temperature for 20 min. Char nanostructure was studied using a Jeol 2200fs operated at 200 keV, equipped with an Oxford Instruments X-Max SDD EDS detector. The curvature of a single graphene sheet is defined in equation 3:

$$Curvature = \frac{Length}{Fiber\ \ length} \tag{3}$$

The length is a straight line that connects both ends of a graphene sheet. The fiber length is the contour or arc length, as shown in the supplemental material (Figure S-1). Both length and fiber length were estimated by Gatan Digital Micrograph software according to the method of Müller et al. [38]. Portions of the image with visible graphene layers were magnified to a size of 10 nm x 10 nm, and both length and fiber length were manually determined by the software ruler which draws a straight or contour line to connect both ends of a graphene sheet.

3. Results

3.1. Char reactivity

Figure 3 shows differential weight loss curves (DTG) for CO_2 gasification (40 % by volume) of wood and herbaceous biomass char samples, metallur-

gical coke, biooil char, and the reacted mixture of biooil with pinewood char at 1600°C. Depending on the sample, the DTG curves show both either a single broad peak or a double peak, both of which indicate a heterogeneous char mixture with respect to reactivity [39, 40]. The maximal reaction rates of chars produced in the drop-tube furnace varied significantly from 800 to 900°C, whereas the wheat and alfalfa straw chars were more reactive than the pinewood, beechwood and leached wheat straw chars [41]. In contrast, the CO_2 gasification of all char samples from pyrolysis at 1300°C for 2 and 12 h took place at nearly the same temperature range from 700 to 1050°C. The maximum CO_2 gasification rate of all chars treated at 1600°C in the CO_2 was about 100°C greater than that of char samples from pyrolysis at 1300°C, confirming the previous results of Trubetskaya [42]. The reactivities of chars from pyrolysis at 2400 and 2800°C were nearly identical. Similar tendencies were observed for the oxidation reactivity of char, as shown in the supplemental material (Figure S-2). The pinewood, beechwood and wheat straw chars obtained from pyrolysis at 2800°C exhibited a triple peak, indicating the development of three main components: a reactive carbon constituent, a carbon constituent with intermediate reactivity, and a less reactive carbon structure with reactivity that approaches that of commercial graphite and metallurgical coke. The reactivity of metallurgical coke was similar to that of pinewood char from pyrolysis 2800°C. The results show that differences in heat treatment temperature have more influence on char reactivity than the residence time and feedstock composition, and will be discussed below.

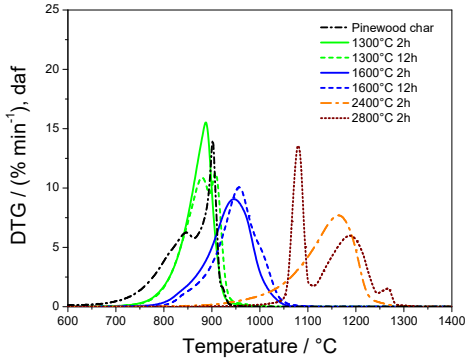

3(a): Pinewood char

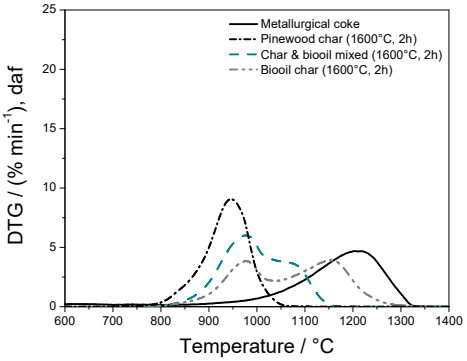

3(b): Reacted biooil with pinewood char

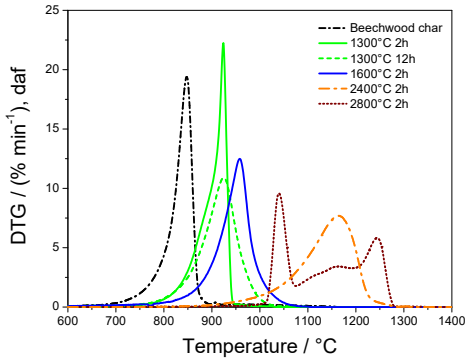

3(c): Beechwood char

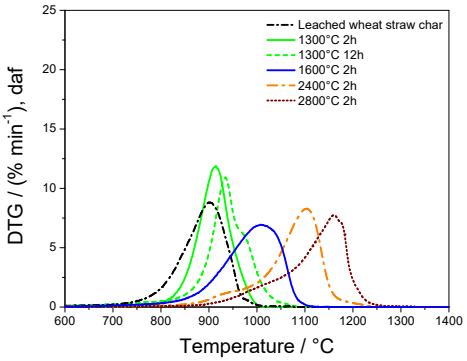

3(d): Leached wheat straw char

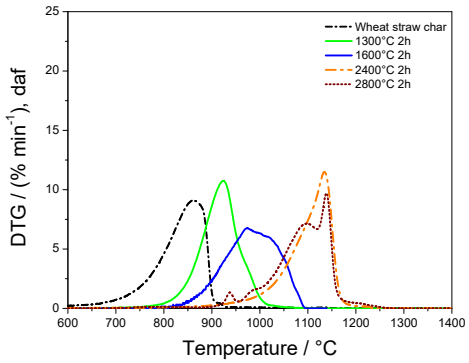

3(e): Wheat straw char

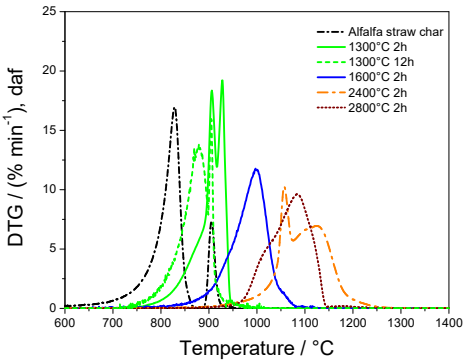

3(f): Alfalfa straw char

Figure 3: (a),(c)-(f) DTG curves of pinewood, beechwood, leached wheat straw, wheat straw, alfalfa straw char from pyrolysis at 1300, 1600, 2400, and 2800°C for 2 and 12 h and (b) DTG curves of pinewood char, mixed pinewood char with biooil, biooil char from pyrolysis at 1600°C for 2 h and metallurgical coke reacted in 40 % volume fraction CO_2 + 60 % volume fraction N_2.

Figure 3(b) shows that the maximum reaction rate of biooil char obtained from pyrolysis at 1600°C was about 100°C greater than that of pinewood char reacted under the same operating conditions, based on the kinetic parameters in the supplemental material (Table S-4). Additional heat treatment of mixed biooil with pinewood char at 1600°C decreased the CO_2 reactivity. The results showed that the maximal CO_2 gasification rate of reacted biooil and pinewood char was about 50°C lower than of metallurgical coke, emphasizing the importance of biooil addition on the char reactivity.

3.2. Elemental analysis

Figure 4 shows a Van Krevelen plot of char derived from wood and herbaceous biomass, metallurgical coke, biooil char, and mixed biooil with pinewood char. The results contained in Figure 4 indicate that the oxygen content in all char samples decreases with the higher heat treatment temperature. The alfalfa straw char obtained from pyrolysis at 1300°C contained less carbon and more oxygen than chars obtained from other feedstocks. Interestingly, the elemental composition of all char samples obtained from pyrolysis at 2400 and 2800°C was comparable to the composition of metallurgical coke.

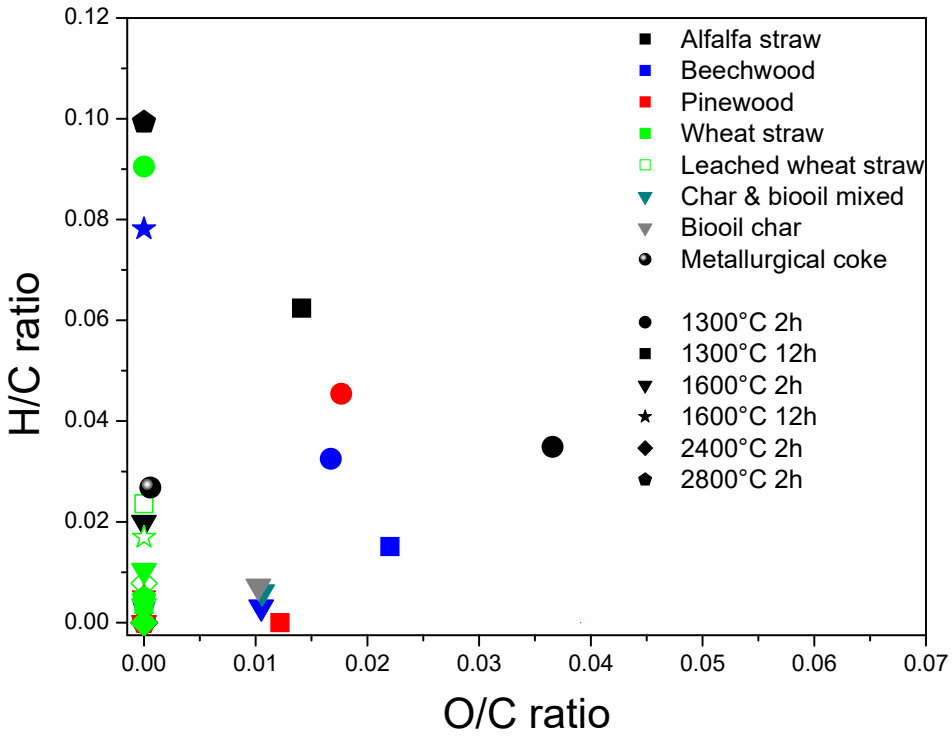

Figure 4: Van Krevelen plot of pinewood, beechwood, leached wheat straw, wheat straw, and alfalfa straw chars from pyrolysis at 1300 and 1600 for 2 and 12 h, 2400 and 2800°C for 2 h, metallurgical coke, biooil char and mixed biooil with pinewood char reacted at 1600°C for 2 h.

3.3. Nanostructure

The nanostructure of the pinewood char treated at 1300 and 1600°C for 2 and 12 h, 2400 and 2800°C for 2 h was studied by TEM, as shown in Figure 5. The pinewood char exhibited a common structure of amorphous carbon at 1300°C, whereas a mixture of amorphous carbon and nano-crystalline graphite was observed at 1600°C. The graphene layers of pinewood char from pyrolysis at 1600°C for 12 h and 2400°C for 2 h were arranged in onion rings

and straight ribbon structures. With increasing residence time, the onion-like carbon structures becomes more prevalent. Increasing the heat treatment temperature up to 2800°C led to the gradual elongation of graphene-like layers and an increased number of graphene segments in the stacks, as shown in Figure 5(f). The pinewood char reacted at 2800°C formed a nanostructure similar to a crystalline carbon membrane [43]. The bent graphene segments of graphitized char contain carbon with hexagonal graphene segments [44] and a mean separation distance of 0.33 nm that indicates the highest degree of graphitization (graphite $\approx$ 0.335 nm) [45]. The pinewood char generated at 1600 and 2400°C had a less ordered structure with the mean separation distance of 0.35 nm. The differences in the nanostructure of pinewood chars generated at 1600 and 2800°C suggest that heat treatment temperature influences the char properties. The long residence time of 12 h at 1600°C led to the formation of ring graphitic structures in pyrolysis of pinewood and beechwood char, as shown in Figure 5(d) and supplemental material (Figure S-21(c)). The less ordered straight graphitic structures were formed at shorter residence times in high-temperature pyrolysis. Figure 6 shows that the biooil char consisted of an amorphous carbon structure, whereas the reacted pinewood char with biooil contained a mixture of amorphous carbon and nano-crystalline graphite structures. The nanostructure of reacted pinewood char and biooil consists of nano-crystalline graphite with 30-50 layers of straight graphene segments. Figure 7 shows the differences in nanostructure of beechwood, leached wheat straw, wheat straw and alfalfa straw chars obtained from pyrolysis at 2800°C.

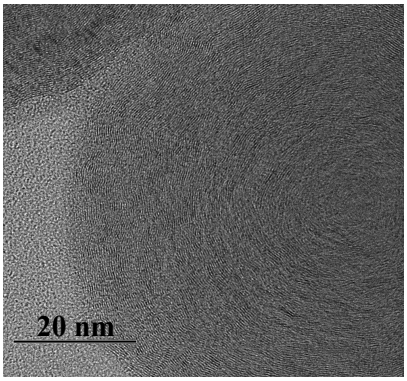

5(a): Pinewood char (1300°C, 2 h)

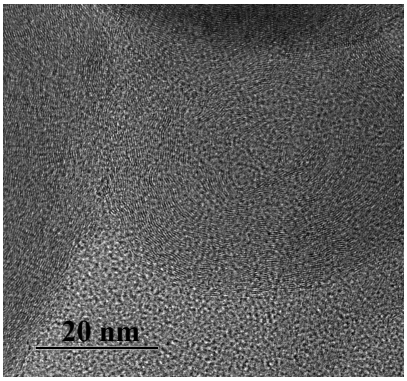

5(b): Pinewood char (1300°C, 12 h)

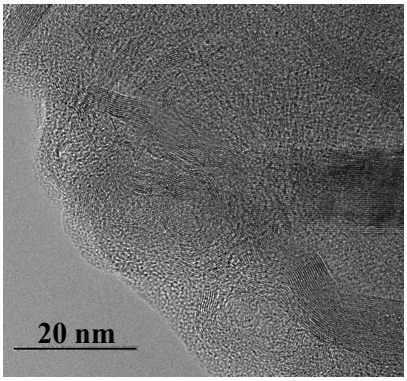

5(c): Pinewood char (1600°C, 2 h)

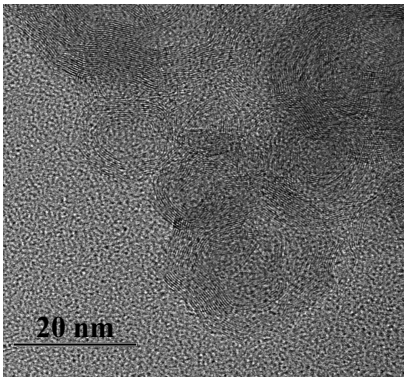

5(d): Pinewood char (1600°C, 12 h)

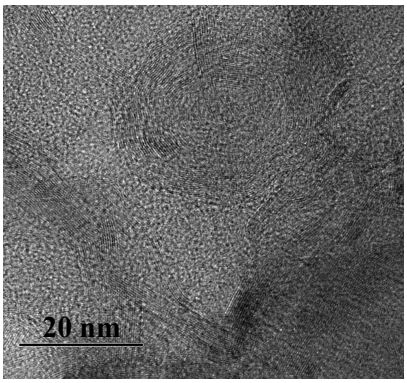

5(e): Pinewood char (2400°C, 2 h)

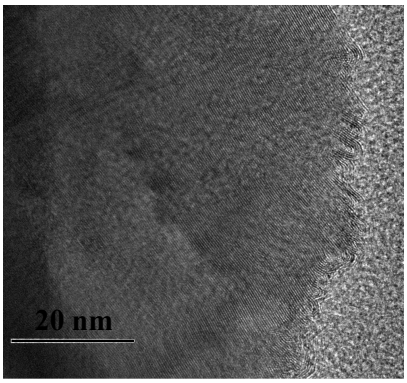

5(f): Pinewood char (2800°C, 2h)

Figure 5: TEM images of pinewood char reacted at 1300°C and 1600°C for 2 and 12 h, 2400 and 2800°C for 2 h.

High heat treatment temperature of pinewood and beechwood chars led to the formation of nano-crystalline graphite with more than 100 layers of straight graphene segments arranged in an interconnected ribbon-like geometry [46]. The leached wheat straw char showed a well-ordered graphitic structure at 1300°C, whereas the wheat straw char exhibited a similar graphitic structure at 2400°C, as shown in the supplemental material (Figures S-22).

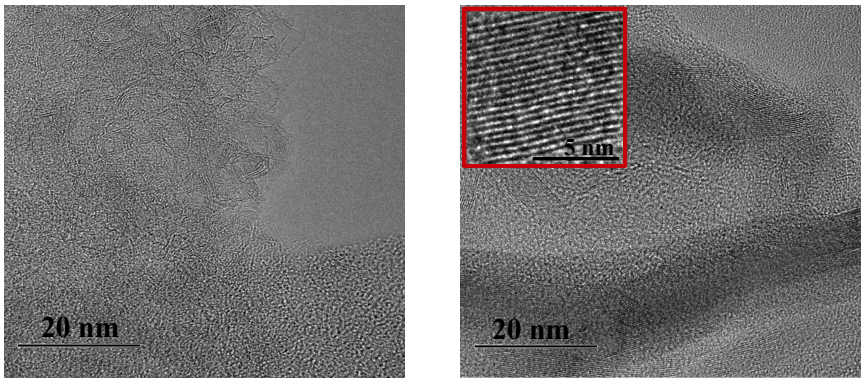

6(a): Biooil char

6(b): Reacted pine char with biooil

Figure 6: TEM images of pyrolyzed biooil and mixed pinewood char with biooil reacted at 1600°C for 2 h. In Figure 6(b) the nano-crystalline graphitic structure is enlarged in the red rectangle.

Differences in carbon structure suggest that leaching of original wheat straw has an influence on the char properties, when the material is treated at temperatures ranging from 1300 to 1600°C. However, Figures 7(b) and 7(c) show that leaching does not affect the char nanostructure at 2800°C, suggesting that temperature becomes the dominant variable at these conditions.

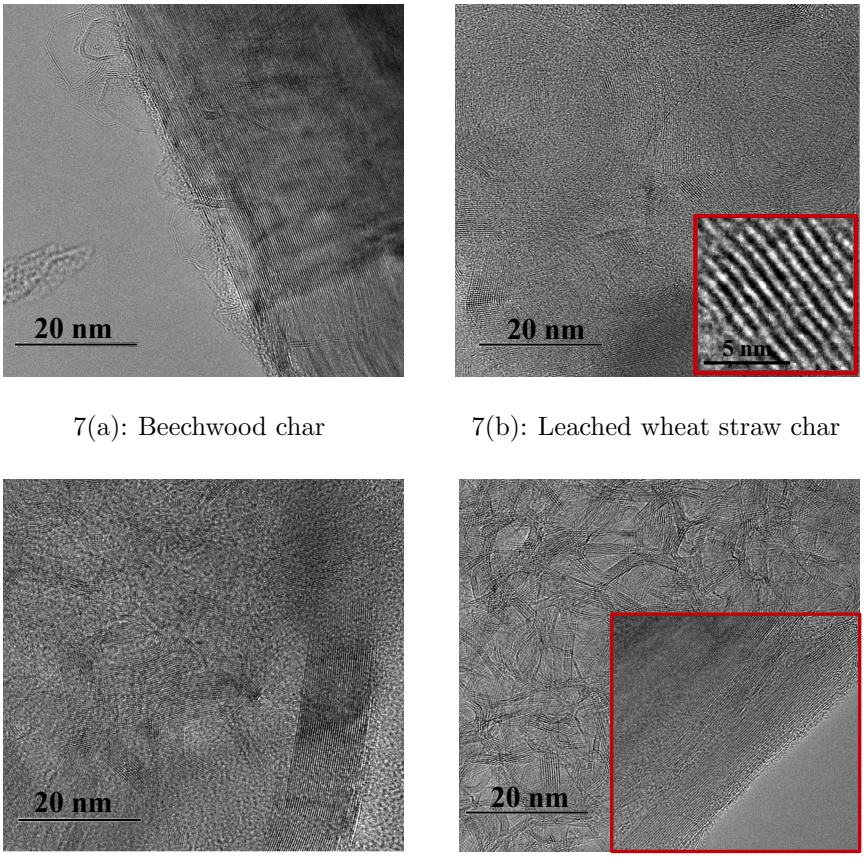

7(a): Beechwood char

7(b): Leached wheat straw char

7(c): Wheat straw char

7(d): Alfalfa straw char

Figure 7: TEM images of beechwood, leached wheat straw, wheat straw, and alfalfa straw char reacted at 2800°C for 2 h. In Figures 7(b) and 7(d) the nano-crystalline graphitic structure is shown in the red rectangle.

313 Both non-treated wheat straw and leached wheat straw chars contained
314 a mixture of an amorphous carbon and a nano-crystalline graphite that was
315 arranged in onion ring structures, similar to the pristine wood and lignin
316 chars [47, 48]. The alfalfa straw char contained a large number of pores up

to around 10 nm long and 5-10 layers thick. The alfalfa straw char structure is mainly composed of curved and faceted nano-crystallites, similar to glassy carbon [49]. The wood chars exhibited a well-ordered graphitic structure, whereas the nanostructure of alfalfa straw char was more porous, containing random fragments with 30-50 layers of straight and long graphene segments.

3.4. Raman spectroscopy

Raman spectroscopy was carried out to examine primary differences in the carbon structure of char samples, as shown in the supplemental material (Figures S-15-S-20). Based on estimated A_D/A_G ratios, all samples exhibited a common structure of amorphous carbon and nano-crystalline graphite, as discussed by Ferrari and Robertson [50]. Pyrolysis at 1300 and 1600°C resulted in a less graphitic char structure (A_D/A_G: 1.1-2.5) than pyrolysis at 2400 and 2800°C (A_D/A_G: 0.4-0.9). The A_D/A_G ratios of pinewood and leached wheat straw chars reacted for 2 or 12 h varied only slightly at 1300 and 1600°C, indicating that the residence time had less influence on the char graphitization than the heat treatment temperature. The biooil char obtained a similar structure to pinewood char and mixed biooil with pinewood char reacted at 1600°C for 2 h with the A_D/A_G ratio of 1.1. The average extension of graphene layers (L_a) in the char reacted at 1300 and 1600°C (2.2-4 nm) was less than those in chars from pyrolysis at 2400 and 2800°C (4.8-10.9 nm). The size of one aromatic ring is 0.25 nm [51], and therefore, the size of PAHs in the char (1300-1600°C) is equivalent to approximately 9-16 aromatic rings and at higher temperatures the amount of aromatic rings increases up to 19-44. The average extension of graphene stacks (L_a) in char samples obtained from pyrolysis at 1300-1600°C was quantitatively similar to

that of commercial carbon black (Printex XE2: 2.5 nm; Vulcan XC72: 2 nm; Printex L: 1.4 nm). Treatment at higher temperatures led to the formation of more graphitic char structure with an average extension similar to graphite (5.6 nm) [52].

4. Discussion

The thermogravimetric experiments showed that heat treatment temperature exerted greater influence on the intrinsic reactivity of char samples than either residence time or feedstock origin. The reactivity of char can be affected by differences in ash composition, residence time, carbon chemistry, nanostructure, and heat treatment temperature. The ash content of native wheat straw (4.1 wt. %) was 20 times higher than that of native pinewood (0.3 wt. %). Thus, based on ash content alone it might be expected that wheat straw char should be more reactive than the pinewood char. However, differences in reactivity were observed only for chars reacted in the drop tube furnace, whereas the reactivities of all chars remained similar at both temperatures (1300 or 1600°C) reacted for 2 and 12 h. This indicates that neither ash composition nor residence time has a strong influence on the observed differences in char reactivity.

The heat treatment temperature, carbon chemistry, and nanostructure of char samples were the main factors influencing the reactivity during CO_2 gasification and oxidation. Raman spectroscopy results showed that all char samples obtained from pyrolysis at 1300 and 1600°C for 2 and 12 h exhibited a structure similar to carbon black based on their comparable A_D/A_G ratios (1.7-2.6). Treatment at higher heat treatment temperatures decreased the in-

tegrated peak area ratios to lower values (0.4-0.9) due to the effects of increasing carbon graphitization. Previous studies showed that low separation distances (close to that of graphite) and high periodicity lead to lower oxidation of carbon materials, while the more bent graphene layers might enhance the reactivity [53, 54]. The char samples exhibit shorter and less curved graphene layers and less recognizable crystalline structure than coal char, indicating either higher porosity or larger fraction of amorphous carbon [55, 56]. This indicates that biomass chars might consist of non-graphitizing carbons [57, 58]. The present results showed that the graphitization of all char samples increases significantly with increasing heat treatment temperature, whereas the CO_2 and O_2 reactivity decreases. The TEM analysis showed that the mean separation distance of graphene segments of chars from pyrolysis at 2400 and 2800°C was similar to graphite (0.335 nm), whereas char samples reacted at 1300 and 1600°C mostly contained an amorphous carbon with a minority component of nano-crystalline graphite. The short graphene layers of chars from pyrolysis at 1300 and 1600°C were associated with higher CO_2 and O_2 reactivity, whereas straight and long graphene segments, which are arranged in more than 100 layers in the char samples from higher temperature pyrolysis, decreased the char reactivity. The results indicated that the composition of original feedstock has an influence on the formation of nano-crystalline carbon in char samples. The nanostructure of alfalfa straw char obtained from pyrolysis at 2800°C was less graphitic and more porous with 30-50 layers of graphene segments than the pinewood char. The long and straight graphene layers of alfalfa straw char at 2800°C suggest that an increase in heat treatment temperature might lead to further char graphitiza-

tion and formation of additional graphene segments, as shown in Figure 7(d). Both pinewood and beechwood chars contained a nano-crystalline graphite with more than 100 layers of straight graphene segments, forming a continuous surface merged with the small fraction of remaining amorphous carbon. The TEM results showed that both woody and herbaceous biomass chars most likely exhibit a graphitizing carbon structure, based on the comparison with the carbon structures proposed by Franklin [55].

The pinewood char obtained from pyrolysis at 1600°C was 59 times more reactive than metallurgical coke in CO_2 gasification. The pyrolysis of biooil led to the formation of less reactive char than pinewood char under similar operating conditions, but still more reactive than metallurgical coke by factor of 27. The reaction rate of the biooil and pinewood char mixture reacted at 1600°C was 15 times greater than that of metallurgical coke, consistent with previous results of Veksha et al. [26]. According to previous reports, the addition of biooil to the pinewood char leads to the formation of carbon deposits during pyrolysis [59, 60]. Thermal decomposition generates H/O/OH radicals that penetrate deep into the char structure, promoting condensation reactions between the PAH rings, forming small ring structures (3-5 fused rings), and later transforming into larger PAH compounds [61, 62]. Carbon deposits consisting of large PAH compounds are difficult to be cleaved during CO_2 gasification, decreasing the char reactivity as observed here and elsewhere [27]. This indicates that both heat treatment temperature and addition of biooil decrease CO_2 gasification reactivity. The elemental composition of metallurgical coke and chars obtained from pyrolysis at 2400 and 2800°C was similar, yielding pinewood char with reactivity comparable to

metallurgical coke. This emphasizes that heat treatment temperature is the most important factor determining CO_2 gasification reactivity. The reaction rates of all char samples treated at 2400 and 2800°C were of the same order of magnitude in CO_2 gasification due to the extent of graphitization of char structure. Raman data were examined to understand the relationship between char reactivity and structure. As shown in Figure 8, the A_D/A_G ratios estimated from Raman spectroscopy were correlated with the CO_2 gasification reactivity.

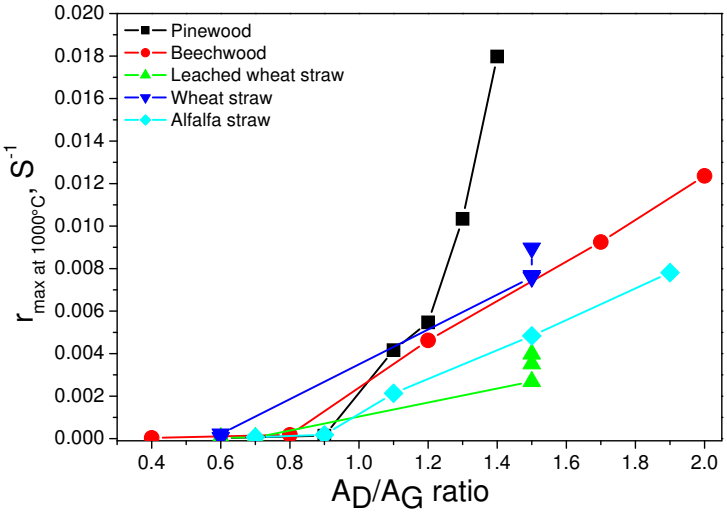

Figure 8: Maximal reaction rate at 1000°C (results from Tables S-4-S-6) during CO_2 gasification versus A_D/A_G ratio of pinewood, beechwood, leached wheat straw, wheat straw, alfalfa straw chars from pyrolysis at 1300, 1600, 2400 and 2800°C for 2 or 12 h (results from Figures S-15-S-20).

Ragardless of source, A_D/A_G ratios are greater than 1 and reactivity is greater than $0.002\,s^{-1}$ for samples treated at temperatures < 2400°C. For A_D/A_G ratios greater than 1, the relationship between A_D/A_G ratios and

reactivity is weak, with feedstock showing a clear impact on reactivity. On the other hand, pyrolysis of all tested materials at temperatures $> 2400°C$ leads to A_D/A_G ratios less than 1 (0.4-0.9) and reactivity less than $0.002\,s^{-1}$. This result clearly demonstrates that treatment temperature becomes the dominating factor governing reactivity when it is greater than 2400°C, with chars obtained from all sources approaching a similar graphitic structure.

5. Conclusion

Various types of biomass were converted into renewable carbonaceous solids by pyrolysis treatment. The resulting materials were studied for reactivity and structure. Thermogravimetric analysis results showed that the CO_2 and O_2 char reactivities depend mainly on heat treatment temperature, and less on the ash composition of the original feedstocks and residence time. Differences in reactivity were ascribed in part to differences in char nanostructure, as evaluated by Raman spectroscopy. Treatment of biochar samples at temperatures greater than 1300°C clearly showed that residual alkali metals have significantly less catalytic influence on char properties than observed at treatment temperatures less than 1300°C. Under properly selected treatment conditions (e.g. $> 2400°C$), chars can be produced from renewable sources with reactivity approaching that of fossil-based metallurgical coke. Co-pyrolysis of biomass with biooil also shows promise for producing carbons with reactivity comparable to metallurgical coke. The finding of this study emphasize the potential use of biocarbon-based reductants in the ferroalloy industries, with concomitant reduction in CO_2 emissions.

Acknowledgements

The authors gratefully acknowledge financial support from the Björn Wahlströms, Kempe Foundation, and Jernkontoret Stiftelsen. M.T. Timko thanks the U.S. National Science Foundation (Grant CBET-1605916). The authors acknowledge the facilities and technical support of Dr. Andras Gorzsas and Dr. Markus Broström at Umeå University. The German Federal Government, Federal State of Nordrhein-Westfalen, Deutsche Forschungsgemeinschaft (DFG) are acknowledged for their contribution toward the establishment of the Interdisciplinary Center for Analytics on the Nanoscale in the University of Duisburg-Essen. BTG Bioliquids in Netherlands is acknowledged for the pinewood biooil supply. Professor Manuel Garcia-Perez is acknowledged for the many fruitful discussions.

References

[1] Holappa L, Towards sustainability in ferroalloy production, J South African Inst Min Metal 110 (12) (2010) 1–8.

[2] Liu J, Chen Z, Ma W, Wei K, Ding W, Application of a Waste Carbon Material as the Carbonaceous Reductant During Silicon Production, Silicon (2018) 1–9.

[3] Monsen B, Tangstad M, Midtgaard H, Use of charcoal in silicomanganese production, 10^{th} Int Ferroalloys Congress INFACON X. Transformation through Technology 68 (2004) 155–64.

[4] Raanes O, Kolbeinsen L, Byberg JA, Statistical analysis of properties for coals used in the production of silicon rich alloys, 8^{th} Int Ferroalloys

Congress INFACON X. Transformation through Technology (1998) 116–20.

[5] Sahajwalla V, Dubikova M, Khanna R, Reductant characterisation and selection: implications for ferroalloys processing, 10^{th} Int Ferroalloys Congress INFACON X. Transformation through Technology 68 (2004) 351–62.

[6] Pistorius PC, Reductant selection in ferro-alloy production: The case for the importance of dissolution in the metal, J South African Inst Min Met 1 (2002) 33–6.

[7] Yoshida T, Turn SQ, Russell SY, Antal MJ, Banagrass vs Eucalyptus Wood as Feedstocks for Metallurgical Biocarbon, Ind Eng Chem Res 47 (2008) 9882–8.

[8] Lundgren M, Blast Furnace Coke Properties and the Influence on Off-gas Dust. Licentiate thesis, Luleå University of Technology, 2010.

[9] Wesenbeeck SV, Wang L, Ronsse F, Prins W, Skreiberg Ø, Charcoal "Mines" in the Norwegian Woods, Energy Fuels 30 (2016) 7959–70.

[10] Wiklund CM, Pettersson F, Saxen H, Optimal Resource Allocation in Integrated Steelmaking with Biomass as Auxiliary Reductant in the Blast Furnace, ISIJ Int 52 (1) (2012) 35–44.

[11] Suopajärvi H, Bioreducer use in blast furnace ironmaking in Finland. PhD thesis, University of Oulu, 2014.

[12] Antal MJ, Grønli M, The art, science, and technology of charcoal production, Ind Eng Chem Res 42 (2003) 1619–40.

[13] Bourke J, Manley-Harris M, Fushimi C, Dowaki K, Nunoura T, Antal MJ, Do All Charcoals Have the Same Chemical Structure? 2. A Model of the Chemical Structure of Carbonized Charcoal, Ind Eng Chem Res 46 (18) (2007) 5954–67.

[14] Griessacher T, Antrekowitsch J, Steinlechner S, Charcoal from agricultural residues as alternative reducing agent in metal recycling, Biomass Bioenergy 39 (2012) 139–46.

[15] Wang L, Skreiberg Ø, Grønli M, Specht GP, Antal MJ, Is elevated pressure required to achieve fixed-carbon yield of charcoal from biomass? Part 2. The importance of particle size, Energy Fuels 27 (2013) 2146–2156.

[16] Brewer CE, Chuang VJ, Masiello CA, Gonnermann H, Gao X, Dugan B and etc., New approaches to measuring biochar density and porosity, Biomass Bioenergy 66 (2014) 176–85.

[17] Zeng K, Minh DP, Gauthier D, Weiss-Hortala E, Nzihou A, Flamant G, The effect of temperature and heating rate on char properties obtained from solar pyrolysis of beechwood, Biores Tech 182 (2015) 114–9.

[18] Smith MW, Dallmeyer I, Johnson TJ, Brauer CS, McEwen JS, Espinal JF and etc., Structural analysis of char by Raman spectroscopy: Improving band assignments through computational calculations from first principles, Carbon 100 (2016) 678–92.

[19] Niksa S, Predicting the rapid devolatilization of diverse forms of biomass with bio-Flashchain, Proc Combust Inst 28 (2) (2000) 2727–33.

[20] Yamagishi K, Endo K, Saga J, A comprehensive analysis of the furnace interior for high-carbon ferrochromium, 1^{th} Int Ferroalloys Congress INFACON 74. Transformation through Technology (1974) 143–7.

[21] De Waal A, Barker IJ, Rennie MS, Klopper J, Groeneveld BS, Electrical Factors Affecting the Economic Optimization of Submerged-arc Furnaces, 6^{th} Int Ferroalloys Congress INFACON 6. Transformation through Technology 1 (1974) 247–52.

[22] Zhao Y, Feng D, Zhang Y, Huang Y, Sun S, Effect of pyrolysis temperature on char structure and chemical speciation of alkali and alkaline earth metallic species in biochar, Fuel Process Tech 141 (2016) 54–60.

[23] Trubetskaya A, Hofmann Larsen F, Shchukarev A, Ståhl K, Umeki K, Potassium and soot interaction in fast biomass pyrolysis at high temperatures, Fuel 225 (2018) 89–94.

[24] Feng D, Zhao Y, Zhang Y, Sun S, Catalytic effects of ion-exchangeable K^+ and Ca^+ on rice husk pyrolysis behavior and its gas-liquid-solid product properties, Energy 152 (2018) 166–77.

[25] Huang Y, Kudo S, Norinaga K, Amaike M, Hayashi I, Selective production of light oil by biomass pyrolysis with feedstock -mediated recycling of heavy oil, Energy Fuels 26 (1) (2012) 256–64.

[26] Veksha A, McLaughlin H, Layzell DB, Hill JM, Pyrolysis of wood to biochar: Increasing yield while maintaining microporosity, Biores Tech 153 (2014) 173–9.

[27] Feng D, Zhao Y, Sun S, Effects of H_2O and CO_2 on the homogeneous conversion and heterogeneous reforming of biomass tar over biochar, Int J Hydrogen Energy 42 (2017) 13070–84.

[28] Trubetskaya A, Brown A, Tompsett GA, Timko MT, Umeki K, Kling J and etc., Characterization and reactivity of soot from fast pyrolysis of lignocellulosic compounds and monolignols, Applied Energy 212 (2018) 1489–500.

[29] Sluiter A, Hames B, Ruiz R, Scarlata C, Sluiter J, Templeton D et al., Determination of Structural Carbohydrates and Lignin in Biomass. Golden (CO): National Renewable Energy Laboratory; 2011 July Report No. NREL/TP-510-42618. Contract No.: DE-AC36-08-GO28308 .

[30] Willför S, Hemming J, Leppänen AS, Analysis of extractives in different pulps - Method development, evaluation, and recommendations. Finland: Åbo Akademi University, Laboratory of Wood and Paper Chemistry; 2004-2009 Report No. B1 of the EU COST E41 action "Analytical tools with applications for wood and pulping chemistry" .

[31] Hames B, Ruiz R, Scarlata C, Sluiter J, Sluiter A, Preparation of Samples for Compositional Analysis. Golden (CO): National Renewable Energy Laboratory; 2011 June Report No. NREL/TP-510-42620. Contract No.: DE-AC36-99-GO10337 .

[32] Thammasouk K, Tandjo D, Penner MH, Influence of Extractives on the Analysis of Herbaceous Biomass, J Agric Food Chem 45 (1997) 437–43.

[33] Coats AW, Redfern JP, Kinetic Parameters from Thermogravimetric Data, Nature 201 (1964) 68–9.

[34] Eilers PHC, Parametric time WarpIng, Analyt Chem 76 (2) (2004) 404–11.

[35] Savitzky A, Golay MJE, Smoothing and differentiation of data by simplified least squares procedures, Analyt Chem 36 (8) (1964) 1627–39.

[36] Sadezky A, Muckenhuber H, Grothe H, Niessner R, Pöschl U, Raman spectroscopy of soot and related carbonaceous materials: Spectral analysis and structural information, Carbon 43 (2005) 1731–42.

[37] Matthews MJ, Pimenta MA, Dresselhaus G, Origin of dispersive effects of the Raman D band in carbon materials, Phys Rev B 59 (10) (1999) R6585–88.

[38] Müller JO, Su DS, Wild U, Schlögl R, Bulk and surface structural investigations of diesel engine soot and carbon black, Phys Chem Chem Phys 9 (2007) 4018–25.

[39] Zolin A, Reactivity of solid fuels. PhD thesis, Technical University of Denmark, 2001.

[40] Meszaros E, Jakab E, Varhegyi G, Bourke J, Manley-Harris M, Nunoura T and etc., Do All Carbonized Charcoals Have the Same Chemical Struc-

582 ture? 1. Implications of Thermogravimetry - Mass Spectrometry Mea-
583 surements, Ind Eng Chem Res 46 (18) (2007) 5943–53.

584 [41] Trubetskaya A, Jensen PA, Jensen AD, Steibel M, Spliethoff H, Glarborg
585 P and etc., Comparison of the high temperature chars of wheat straw
586 and rice husk with respect to chemistry, morphology and reactivity,
587 Biomass Bioenergy 86 (2016) 76–87.

588 [42] Trubetskaya A, Fast pyrolysis of biomass at high temperatures. PhD
589 thesis, Technical University of Denmark, 2016.

590 [43] Wollbrink A, Volgmann K, Koch J, Kanthasamy K, Tegenkamp C, Li
591 Y and etc., Amorphous, turbostratic and crystalline carbon membranes
592 with hydrogen selectivity, Carbon 106 (2016) 93–105.

593 [44] Welz S, McNallan MJ, Gogotsi Y, Carbon structures in silicon carbide
594 derived carbon, J Mat Proc Tech 179 (2006) 11–22.

595 [45] Zhang ZL, Brydson R, Aslam Z, Reddy S, Brown A, Westwood A and
596 etc., Investigating the structure of non-graphitising carbons using elec-
597 tron energy loss spectroscopy in the transmission electron microscope,
598 Carbon 49 (2011) 5049–63.

599 [46] Jenkins GM, Kawamura K, Polymeric Carbons - Carbon Fibre, Glass
600 and Char, Cambridge University Press, 1976.

601 [47] Dufour A, Celzard A, Fierro V, Broust F, Courson C, Zoulalian A and
602 etc., Catalytic conversion of methane over a biomass char for hydrogen
603 production: deactivation and regeneration by steam gasification, Appl
604 Cat A: General 490 (2015) 170–80.

[48] Li Y, Hu YS, Chen L, Li H, Huang X, A superior low-cost amorphous carbon anode made from pitch and lignin for sodium-ion batteries, J Mat Chem A 4 (2016) 96–104.

[49] Jurkiewicz K, Pawlyta M, Zygadlo D, Chrobak D, Duber S, Wrzalik R and etc., Evolution of glassy carbon under heat treatment: correlation structure-mechanical properties, J Mater Sci 53 (2018) 3509–23.

[50] Ferrari AC, Robertson J, Raman spectroscopy of amorphous, nanostructured, diamond-like carbon, and nanodiamond, Phil Trans R Soc Lond 362 (2004) 2477–512.

[51] Hayashida K, Nagaoka S, Ishitani H, Growth and oxidation of graphitic crystallites in soot particles within a laminar diffusion flame, Fuel 128 (2014) 148–54.

[52] Jawhari T, Roid A, Casado J, Raman spectroscopic characterization of some commercially available carbon black materials, Carbon 33 (11) (1995) 1561–5.

[53] Hurt RH, Structure, properties, and reactivity of solid fuels, 27^{th} Symposium on Combust (1998) 2887–904.

[54] Liati A, Eggenschwiler PD, Schreiber D, Zelenay V, Ammann M, Variations in diesel soot reactivity along the exhaust after-treatment system, based on the morphology and nanostructure of primary soot particles, Combust Flame 160 (3) (2013) 671–81.

[55] Franklin RE, Crystallite Growth in Graphitizing and Non-Graphitizing Carbons, Proc R Soc A Math Phys Eng Sci 209 (1951) 196–218.

[56] Bar-Zic E, Zaida A, Salatino P, Senneca O, Diagnostics of carbon gasification by Raman microprobe spectroscopy, Proc Combust Inst 28 (2000) 2369–74.

[57] Oberlin A, Carbonization and graphitization, Carbon 22 (6) (1984) 521–41.

[58] Kurosaki F, Ishimaru K, Hata T, Bronsveld P, Kobayashi E, Imamura Y, Microstructure of wood charcoal prepared by flash heating, Carbon 41 (15) (2003) 3057–62.

[59] Appleby W, Gibson J, Good G, Coke formation in catalytic cracking, Ind Eng Chem Pro Des Dev 1 (1962) 102–10.

[60] Coll R, Salvado J, Farriol X, Montane D, Steam reforming model compounds of biomass gasification tars: conversion at different operating conditions and tendency towards coke formation, Fuel Process Technol 74 (2001) 19–31.

[61] Tay HL, Kajitani S, Zhang S, Li CZ, Effects of gasifying agent on the evolution of char structure during the gasification of Victorian brown coal, Fuel 103 (2013) 22–8.

[62] Keown DM, Hayashi JI, Li CZ, Drastic changes in biomass char structure and reactivity upon contact with steam, Fuel 87 (2008) 1127–32.